Hindawi
Journal of Sensors
Volume 2019, Article ID 1864239, 11 pages
https://doi.org/10.1155/2019/1864239

Research Article

Shear-Force Sensors on Flexible Substrates Using Inkjet Printing

Andreas Albrecht,[1] **Mauriz Trautmann**,[1] **Markus Becherer**,[1] **Paolo Lugli**,[2] **and Almudena Rivadeneyra**[2]

[1]*Institute for Nanoelectronics, Technical University of Munich, Arcisstraße 21, 80333 Munich, Germany*
[2]*Free University of Bozen-Bolzano, Universitätsplatz 1 39100 Bozen-Bolzano, Italy*

Correspondence should be addressed to Andreas Albrecht; Andreas.albrecht@tum.de

Received 10 August 2018; Accepted 24 December 2018; Published 3 March 2019

Academic Editor: Franz L. Dickert

Printing techniques are a promising way of fabricating low-cost electronics without the need for masking and etching. In recent years, additive printing techniques, such as inkjet and screen printing, have been adopted to fabricate low-cost and large-area electronics on flexible substrates. In this work, a three-axial normal and shear force sensor was designed and printed that consists of four miniaturized, printed capacitors. The partially overlapping electrodes are arranged in a manner, so that force sensitivity in orthogonal directions is achieved. A silicone rubber is used as an elastic dielectric and spacer between the two electrodes. The base unit of this sensor has been fabricated using inkjet printing and characterized for normal and shear forces. The force response was investigated in a force range from 0.1 N to 8 N, the normal-force sensitivity was determined to be Sz = 5.2 fF/N, and the shear-force sensitivity was Sy = 13.1 fF/N. Due to its sensing range, this sensor could be applicable in tactile sensing systems like wearables and artificial electronic skins.

1. Introduction

Printed electronics possess the advantage of reducing the number of production steps by applying several components with similar process technologies. In contrast to conventional electronics manufacturing, sensors can be printed instead of assembled [1–3]. The present work deals with the development, fabrication, and characterization of a capacitive normal and shear force sensor. Such sensors could be used for basic force and pressure measurements [4, 5]. They could also be part of a tactile sensing system in robotics. Advanced robotic systems need reliable information about friction and strain when interacting with the environment and while handling objects [6–9]. Additionally, the ability of printed electronics to fabricate devices on flexible substrates could bring us a step closer to an artificial skin, which can be wrapped around the robot's surface [9–14].

In a previous work, we studied inkjet printing and photonic sintering for low-cost printing of electrodes and wiring [15]. Inkjet printing is able to print lines down to about 60 μm in width and can be conducted on a large range of flexible and low-cost substrates. Photonic sintering is a method that allows achieving highly conductive thin films on temperature-sensitive substrates with conductivities of up to 40% of the bulk conductivity [15] Therefore, these two technologies are well suited for the production of electrodes for sensors.

In this work, we want to focus on a capacitive three-axial shear-force sensor as an alternative to resistive force sensors [16, 17] that is applicable in an artificial skin. A common approach for building capacitive flat force sensors are the use of two parallel plates that change their distance upon pressure [9, 18, 19]. The gap can be air-filled [20] or consist of an elastic dielectric [21]. Lee et al. [20] have modified this principle to additionally recognize shear forces by introducing several capacitors.

Several research groups have tried to produce thin-film three-axial force sensors. Chase and Luo [22] showed a parallel plate capacitor approach with four capacitances that change in the overlapping area for exposure to shear forces and in distance for normal forces. Khan et al. [23] presented an all-screen printed flexible pressure (normal force) sensor

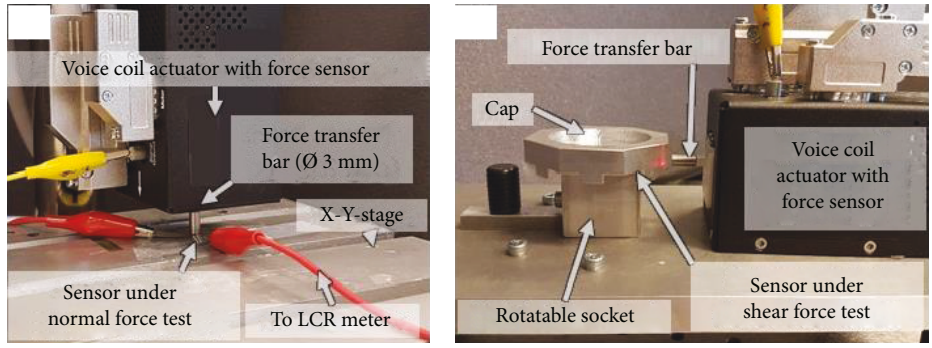

(a) (b)

Figure 1: Measurement setup for (a) normal forces and (b) shear forces. The metallic bar transfers the force generated by the voice coil actuator to the sensor and the cap where the sensor is fixed, respectively.

with a piezoelectric sensing principle. In their work, silver- (Ag-) based paste serves as a conductor for the electrodes. The piezoelectric material was polyvinylidene fluoride trifluoroethylene (P(VDF-TrFE)), which is a ferroelectric polymer that exhibits efficient piezoelectric and pyroelectric properties. The force response was characterized by the voltage readout.

A thin-film normal and shear force sensor was designed by Viry et al. [24] as well as Chase and Luo [22]. Their capacitive device senses normal and shear forces simultaneously. The operation is based on the deflection of a compressible filler material, which is sandwiched between two electrodes of a plate capacitor. Making a few adjustments, this design could be implemented using printing technologies.

A more advanced sensor design was reported by Dobrzynska and Gijs [25] using conventional semiconductor technology. Their capacitive approach is based on the deflection of an elastic dielectric spacer. They used multiple small capacitor areas leading to a higher sensitivity especially for shear force sensing. However, the fabrication of similarly small features is a challenging task using printed electronics techniques. A similar approach was used by Surapaneni et al. [26] who also developed a portable readout device.

In the present work, the basic idea of their sensor was adopted for printed electronics. The rest of the paper is structured as follows: in Section 2, we present the materials, the printing process, the elastic dielectric, and its application as well as the characterization tools used to produce the presented results. Section 3 discusses the design, a theoretical model thereof as well as the evaluation of the print quality and the measured electromechanical behavior of out sensors. In Section 4, we summarize the main findings and conclude the paper.

2. Materials and Methods

The shear-force sensors were fabricated on the transparent, coated Polyethylene Terephthalate (PET) film Screenfilm Waterbased (ColorGATE Digital Output Solutions GmbH, Germany). The film was developed for inkjet printing and has a nanoporous surface coating, a grammage of 210 gm^{-2}, and a thickness of 170 μm.

For inkjet printing, we used the nanoparticle-based silver ink DGP 40LT-15C (ANP Co., South Korea). The ink contains 35% silver nanoparticles dispersed in TGME ($C_8H_{18}O_4$), which is a polar solvent. The dispersion was carefully shaken by hand prior to filling into the cartridge. The curing temperature is indicated with 120-150°C, and the specific resistivity is 11-12 $\mu\Omega$cm. As the dielectric spacer of our sensor, we used a two-component screen-printable silicone paste, Alpatec 30191 (CHT R. Beitlich GmbH). The two components were mixed equally (1 : 1) in a small dish. After mixing, the paste can be used for one hour before hardening. Both components are highly transparent.

2.1. Inkjet-Printed Electrodes. The printer used in this work is a Dimatix DMP-2850 (Fujifilm Dimatix Inc., Santa Clara, USA). The cartridge and plate temperature was set to 55°C with a drop-spacing of 30 μm. This value guarantees a yield rate higher than 90% while the distance between consecutive electrodes is close enough. Reducing this spacing will increase the capacitance and sensitivity of our sensors, but it would reduce the reproducibility of the fabrication. With these settings, the fabrication of one electrode took about ten minutes. By using more than one nozzle, the printing time can be reduced, but the probability of a failure due to a blocking in one of the nozzles is much higher. Through the heat of the platen, the pattern was quickly dried. To make sure that all the solvents evaporated, the samples were additionally cured in an oven for 60 min at 60°C. The substrate limited the temperature as it started to buckle at higher values.

To improve the conductivity of the electrodes, we employed Intense Pulsed Light (IPL) sintering using a Sinteron 2010 (Xenon, US). A double pulse (period of 3 s) at 2.5 kV was used. The pulse lengths were 500 μs for the first pulse and 1000 μs for the second pulse, which were identified as good values in previous work [15]. The manufacturer measured a light intensity of 2.6-3.9 Jcm^{-2} for a single pulse at 830 J of electrical power. Our light intensity for both pulses is assumed to be approximately in this range as the employed pulses are about 300 J and 600 J, respectively.

2.2. Elastic Spacer. The Polydimethylsiloxane (PDMS) spacer was applied onto the inkjet-printed silver layer on the PET

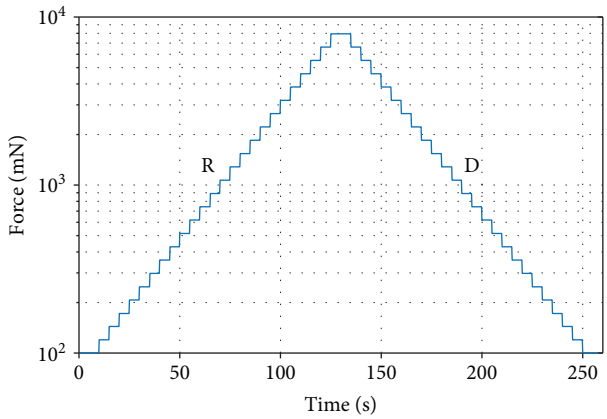

FIGURE 2: Force profile for normal and shear response measurements with increasing (R) force from 100 mN in steps of 20% up to 8 N and decreasing (D) force with the same values.

film using a stencil made of 75 μm thick Kapton film. After applying PDMS on both electrodes, they were placed on each other, aligned using dedicated marks, and baked on a hot plate at 60°C for about 30 min. To make sure that the electrodes did not detach, a slight pressure was exerted on the sample using a glass slide. In this way, we effectively used the PDMS as both an adhesive as well as a dielectric spacer of our sensor.

2.3. Characterization. Optical microscope images were taken with a Zeiss Germany Axio Lab.A1, equipped with a digital camera Axiocam 105. These images were used to assess the quality of the printed electrodes and to determine their lateral and longitudinal dimensions. Further, the drop diameter of the silver ink on the PET and Kapton substrates was identified.

The thickness of our printed electrodes and PDMS layer were measured with a DektakXT stylus surface profiler (Bruker Corporation, USA).

To generate the normal and shear force, we used the voice coil linear actuator V-275 PIMag (Physik Instrumente, Germany) with an integrated force sensor. Figure 1(a) shows the actuator mounted to a movable stage for the normal force application. The fabricated sensor was fastened to the table using double-sided adhesive tape. To reduce parasitic capacitive coupling, a 2.5 mm × 2.5 mm glass slide was put between the metallic bar of the motor and the sensor. The capacitance of a fabricated sensor was continuously recorded using an Agilent E4980A Precision LCR Meter (100 kHz, 0 V bias, and 1 V AC voltage). The characterization was automated by a LabVIEW program.

For the shear-force characterization, a different setup was developed and built using the same voice coil actuator. Figure 1(b) shows the measurement setup. The force is applied precisely on the sensor plane, thus parasitic forces are minimized. To characterize the samples from all directions, the socket can be rotated from -90 to +90. One side of the sensor is fixed with a double-sided tape to the socket and the other side to the cap. To route the wiring out, small grooves are milled into the bottom of the cap.

For the electromechanical characterization, we loaded the sensors with forces from 0.1 N to 8 N with incremental steps of 20% every five seconds, and subsequently, the force was reduced by the same factor. This was repeated three times. The time-force signal is shown in Figure 2. For the evaluation of the hysteresis, we differentiated between the rising and the declining edges of the profile. In Figure 2, the rising edges are labeled with R and the declining edges are denoted with D.

3. Results and Discussion

3.1. Sensor Design. The design of the sensor was defined by the requirements and technical capabilities described in the previous sections. Thus, we were looking for a sensor, which can be fabricated on flexible substrates, like Kapton and PET, using inkjet and screen printing.

In literature, different capacitive sensors were demonstrated. For example, Chase and Luo [22] presented a shear and normal force sensor where four squared electrodes form the bottom and a single squared electrode the top of the sensor. The operation was based on the deflection and compression of the filler layer between top and bottom electrodes.

The shear force and direction were then determined by calculating the ratios of the four single capacities. The downside of this configuration is that one only obtains very small delta in the capacitance, especially when measuring shear force. Therefore, the basic principles of the four individual capacitors had to be modified to achieve an improvement in sensitivity.

So, instead of using square electrodes, we chose an "E"-shaped pattern for both the top and the bottom electrode. This approach was presented by Dobrzynka and Gijs in 2013 [25]. Figure 3 shows the proposed design of our sensor that consists of four parallel-plate capacitors C1–C4. Each of them is formed between a finger structure at the bottom that has the size of one of the four squares plus a wiring. The bottom prints are shown in red and the top print is shown in yellow. The overlapping area of the top and the bottom print is shown in orange and the dielectric spacer (PDMS) is shown in beige. The contact pads on the right side are connected to each of the electrodes. They are all on one side and as far away from the sensing area as necessary to be able to contact them outside of our shear-force setup. The central one is connected to another contact pad that exists on both print patterns and links the top and bottom print next to the dielectric layer. We decided to number the capacitance values with the location of the contact pads from top to bottom. Thus, the counting starts with C1 in the top right corner and continues counterclockwise.

Figure 3 shows a magnification of a part of all electrodes on the right side and allows a closer look at the design of the electrodes. Again, the bottom electrodes are shown in red, the top electrodes in yellow, and the overlapping areas in orange. The top right and bottom left electrodes change the overlapping area of the fingers, if a force in the positive or negative x-direction is applied. For positive forces in the x-direction, the overlapping area increases for C1 and decreases for C3 and vice versa for negative forces. The

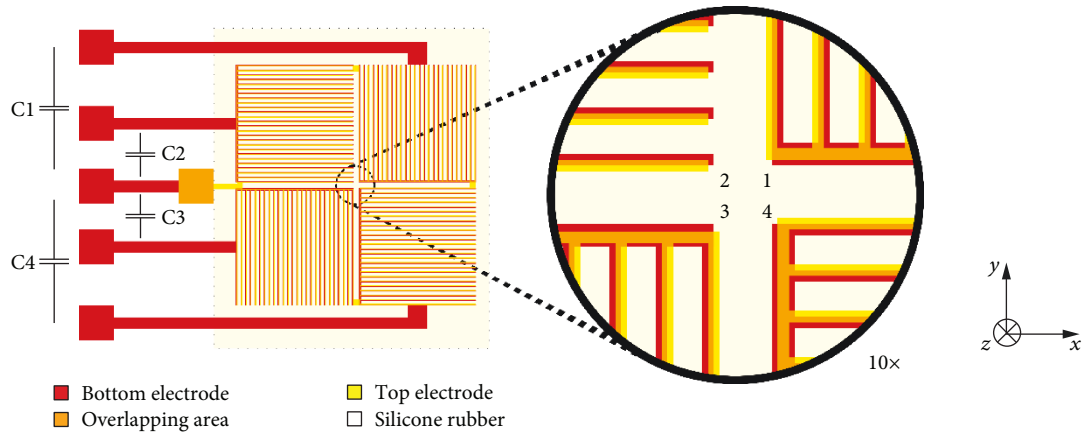

FIGURE 3: Design of our sensor with the four sectors that form the four capacitances $C_1 \ldots C_4$ that allow the differentiation of forces in x-, y-, and z-direction. In every sector, the top and bottom electrode is shifted in a different direction.

maximum allowable shift in the x-direction is half of the electrode width. For shear forces in the positive or negative y-direction, the overlapping area does not change until the same limits because the bottom electrodes are larger than the top ones. The top left (C2) and bottom right (C4) electrodes increase and decrease their overlapping area for a positive force in the y-direction. The tip of the fingers as can be seen in the magnification of C2 is extended for the bottom layer to allow a movement in x-direction without altering the overlap area.

The benefit of these "E"-shaped structures is that one obtains multiple edges, so that a deflection leads to a larger change in the parallel area of the capacitor. The top and bottom electrode are displaced by half of the finger width, so the initial capacitance amounts to 50% of the maximum capacitance. Two of the capacitors are x-axis--sensitive, and the other two are y-axis sensitive.

3.2. Theoretical Model. The sensor was modelled using a simple approach with a parallel-plate capacitor formed by the top and bottom electrodes. An exactly 50% overlap area for the fingers, a 100% overlap of the connection wires between the electrodes, and no influence of the wiring and the pads were assumed. The areas of all four squares were designed identically with the area $A = A_1 = A_2 = A_3 = A_4$. For the theoretical model, it is assumed that the dielectric is equally thick across the entire sensor with a thickness of d. Therefore, the basic parallel plate capacitor formula (1) can be employed for the initial capacitance C_0:

$$C_0 = \varepsilon_0 \varepsilon_r \frac{A}{d}. \tag{1}$$

A force in z-direction reduces the distance by Δd_z, which increases the capacitance of all four capacitors. A force in x-direction increases the area of the capacitor C_1 by ΔA_x and decreases the area of C_3 to the same extent while not influencing C_2 and C_4. The resulting capacitance values are shown in the first equation in (2). Similarly, a force in y-direction increases the overlap area of capacitor C_2 by ΔA_y and decreases the area of C_4 to the same extent and does not alter C_1 and C_3 as shown in the second equation:

$$\begin{aligned} C_{1/3} &= \varepsilon_0 \varepsilon_r \frac{A \pm \Delta A_x}{d - \Delta d_z}, \\ -C_{2/4} &= \varepsilon_0 \varepsilon_r \frac{A \pm \Delta A_y}{d - \Delta d_z}. \end{aligned} \tag{2}$$

The average value of all four capacitances cancels out all area changes caused by the x- and y-forces because we assumed that an area increase of one capacitor is equally compensated by an area decrease of another. The average value only depends on the distance between the parallel plates according to the normal force. This force in the z-direction can be determined by the change of the calculated average capacitance C_z divided by the initial capacitance C_0 as shown in (3). An approximation for small deflection of the top electrodes is given so it shows that for small forces, the behavior is almost linear:

$$C_z = \frac{1}{4} \sum_{n=1}^{4} C_n = C_0 \cdot \frac{d}{d - \Delta d_z} \approx C_0 \cdot \left(1 + \frac{\Delta d_z}{d}\right). \tag{3}$$

The increase or decrease of C_1 and C_3 for a shear force in the positive direction can be expressed in relation to C_z as shown in (4). Similarly, the expression for C_2 and C_4 is to be calculated.

$$C_{1/3} = \left(1 \pm \frac{\Delta A_x}{A}\right) \cdot C_z. \tag{4}$$

A subtraction of each pair of capacitance leads to an expression that reduces the z-dependence and can serve as indicators for the applied shear forces in the x- and y-direction as shown in (5). Each value remains constant for a force in the perpendicular direction because it is only depending on the changes in the area. If the subtraction of the pairs is divided by C_z, the z-direction dependence can be eliminated.

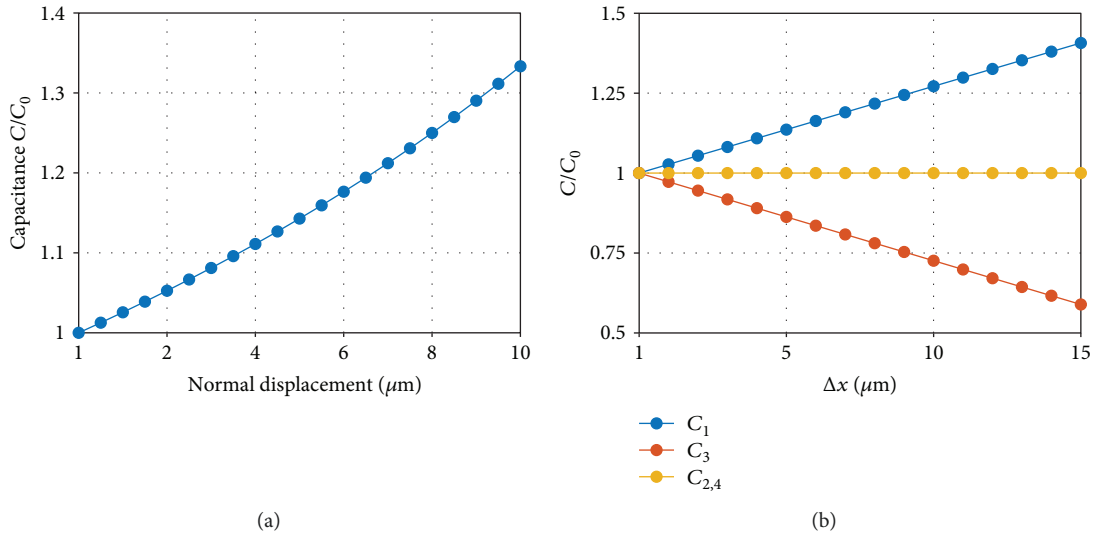

FIGURE 4: Theoretical model of the sensor's response on a displacement due to (a) normal force (z-direction) and (b) shear force in x-direction.

It has to be noted that the typical changes of the capacitance are low. A small noise caused by the measurement of the capacitance can introduce a large error when calculating this division.

$$C_x = \frac{(C_1 - C_3)}{2 \cdot C_z} = \frac{\Delta A_x}{A}, \qquad C_y = \frac{(C_2 - C_4)}{2 \cdot C_z} = \frac{\Delta A_y}{A}. \tag{5}$$

A numerical simulation was conducted to estimate the amount of the capacitance change and the influence of distance reduction to the difference of the capacitance pairs. One capacitor consists of 31 fingers with a width of about 60 μm and a length of 5.95 mm. The connecting bridge has an area of 1.22 μm^2. For the calculations, we took a 40 μm thick dielectric in idle position, and the relative dielectric permittivity of PDMS was taken as 2.5 [27]. The relative change of the capacitance due to a displacement of the top electrode by a certain distance on the impact of a normal force in the z -direction is depicted in Figure 4(a). It can be seen that the change for the capacitance is about linear for a small displacement until about 4 μm, which is 10% of the total dielectric's thickness. At a higher displacement, the capacitance changes at a higher rate according to (4) and is not linear anymore. As PDMS is hardly compressible, we assume that it is a reasonable assumption that the displacement is small enough to still follow a linear curve. Figure 4(b) shows the capacitance normalized to the initial capacitance C_0 for a shear force in the x-direction. As shown in (4), these are linearly dependent on the force-induced area change, which in turn is linear to the displacement. The slope of C_1 is positive with the same absolute slope than C_3, but C_3 is decreasing. A subtraction of C_3 from C_1 results in a linear relation, too.

A change in the normal force affects the change of the shown shear-force behavior. Figure 5 highlights the influence of the normal displacement on the individual capacitor values. Previous work by Dobrzynka and Gijs [25] neglected this effect. However, already small normal forces that compress the dielectric layer by a few percent can lead to a large error, especially when measuring small shear forces. This work suggests calculating the C_x and C_y values according to (5) to reduce this effect.

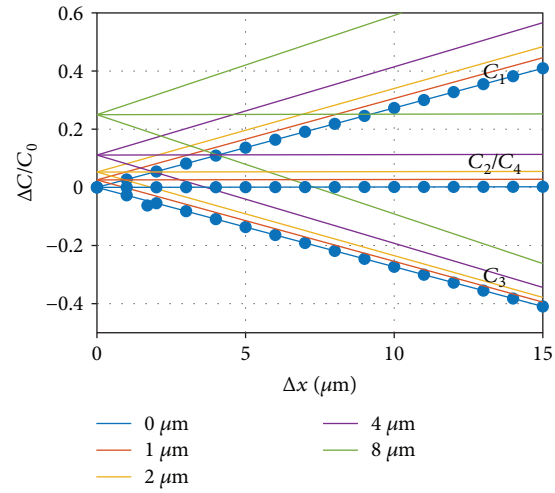

FIGURE 5: Calculated capacitance values for the individual capacitances for a shear load in x-direction at different constant z-forces.

3.3. Print Characterization. We decided to employ inkjet printing as the manufacturing technique for the sensor electrodes because the layer thickness is approximately one order of magnitude smaller than for screen printing. Figure 6 shows the inkjet-printed finger structures for two different finger geometries. On the left, fingers with a width of two drops to ensure the electrical connection even though one drop would not be correctly printed. A gap of three dots was necessary to achieve a suitable distance between the

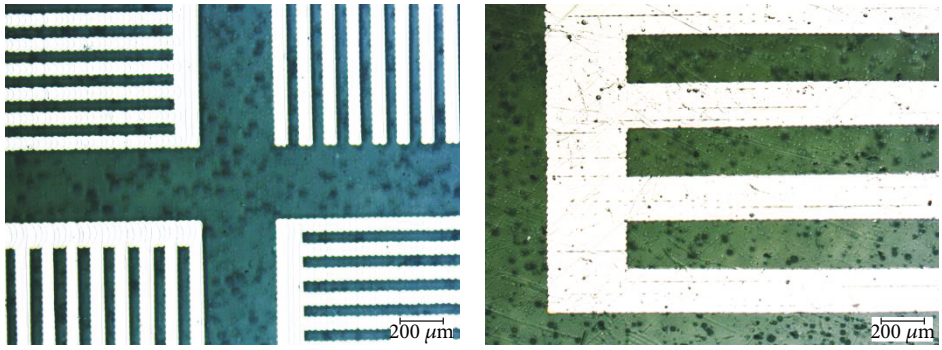

Figure 6: Inkjet-printed electrodes with different finger width of (a) 60 μm and (b) 210 μm. The silver can be seen bright while the substrate is dark. The individual droplets form small bulges on the edges.

fingers. A drop spacing of 20 μm was chosen to be ideal for the repro film (T6). Due to the drop gain of the inkjet-printed drops, the final finger width is about 60 μm and a gap of 40 μm. Still, inkjet printing of the pattern was not reproducible, and we obtained broken fingers on a regular basis. Furthermore, the alignment of the top and bottom electrodes turned out to be more difficult than initially assumed. These were the reasons why we decided to continue the work with larger fingers as shown in Figure 6(b). The finger width is 210 μm and the not perfectly printed areas on the fingers are of minor importance. To still reach relatively high capacitance values, we increased the length of the 22 fingers to 8.8 mm. The average thickness of the thin film forming the electrodes was 412 nm. It is about 1% of the thickness of the 40 μm thick dielectric that was applied by stencil printing on top of the fingers and can be neglected.

The profile measurement shown in Figure 7 was recorded perpendicular to the printing direction. We measured an average thickness of 412 nm. The green markers indicate drop rows where nozzle failure occurred and the thickness of the film is much lower. Since these gaps only appear locally, we expect them to have a small influence on the conductivity of the electrodes. However, the thickness of the silver layer greatly affects the conductivity of the electrodes. At this point, we were not aware of the fact that the conductivity could be a problem for the performance of the sensor.

The top electrode was then aligned on top of the bottom electrode and pressed with the help of a glass slide onto the still wet stencil-printed PDMS without squeezing it out of the defined area. For the first investigation, we built a sensor that only uses one-quarter of the final sensor. Figure 8 shows the assembled quarter of the sensor with the dielectric print across the entire area, except the left side of the photo where a white shadow is perceivable. Especially, the upper electrode, which is the bottom electrode, is shown milky because the employed PET film is milky. On contact with PET, it turns transparent and both electrodes can be clearly seen. The fabricated sensor was then contacted at the rectangular contact pads. Therefore, the overhanging PET foil was cut off, and the contact pads

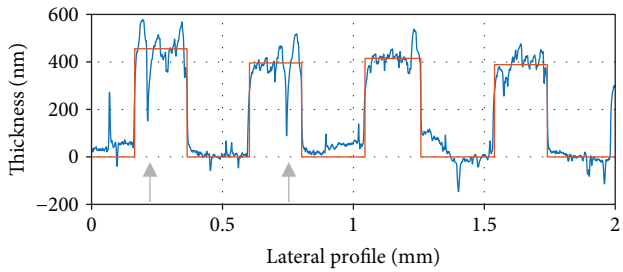

Figure 7: Profile of an inkjet-printed electrode. An average thickness of 412 nm was measured within the red marked areas. The spikes marked by green arrows may lead to an interruption of the conductive path.

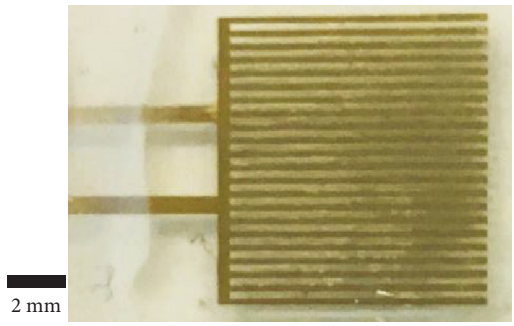

Figure 8: Optical image of one-quarter of the sensor including wiring.

were uncovered. To plug the sensor to the LCR meter, two small wires were attached by conductive epoxy.

3.4. Electromechanical Characterization. The results of the normal force sensing experiments are depicted in Figure 9. The data is collected from one characterization cycle, including three rising and declining force ramps. The blue lines represent the reference force signal and the red lines represent the capacitance signal. It can be seen that the capacitance signal follows the force signal accurately and reaches about 40 fF to 45 fF. A small delay between both signals was found that indicates a hysteresis. Furthermore, the sensor shows a small drift of several femtofarads. This is caused by the viscoelastic behavior of PDMS.

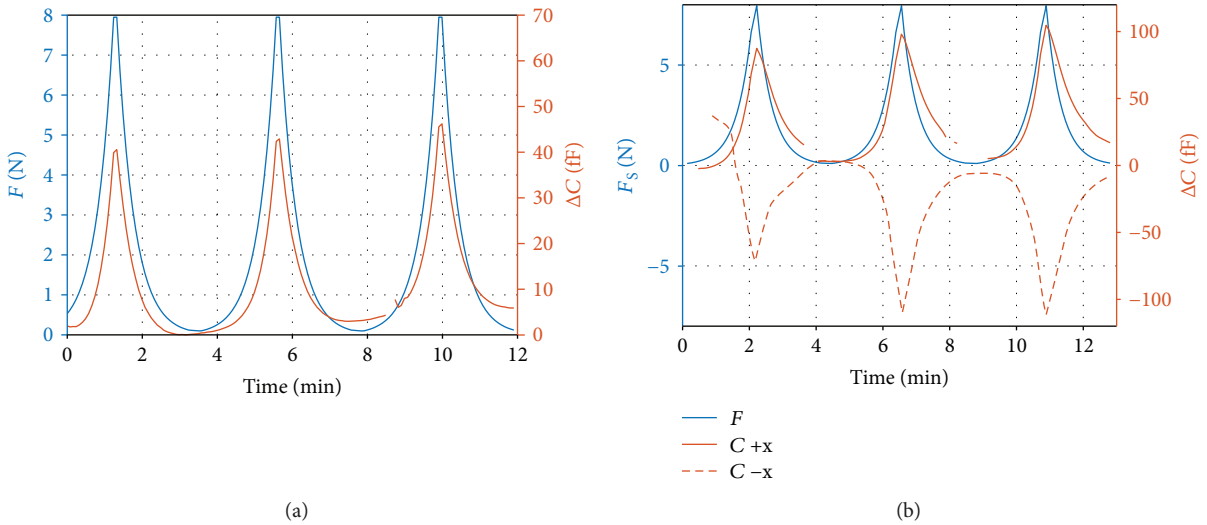

FIGURE 9: (a) Shows the capacitance response (red) to a normal force (blue) over time. (b) The solid red line corresponds to the capacitance change due to a force in $-x$-direction and the dashed line to the $+x$-direction.

The sensor was characterized with our custom-made shear-force setup. The sensor was put below the cap and characterized for shear forces in one direction. Then, the table was turned by 180° and the sensor could be characterized for the opposite force without removing it from the setup. In Figure 9(b), the solid line represents a shear force in -x-direction and the dashed lines a shear force in $+x$ -direction. The negative direction was conducted first and showed a very different behavior to the following cycles. Therefore, we aligned this signal according to the measured capacitance after finishing the first-force ramp. Then, the sensor responses were repeatable for the consecutive two ramps in the negative and three ramps in the positive x -direction. The sensor responses occur almost simultaneously with the application of a shear force, and the amplitudes for both directions are very similar (up to 110 fF and 105 fF for the negative and positive x-direction, respectively).

Due to the viscoelastic relaxation of the PDMS, the capacitance during unloading of the force is slightly higher than at loading. Furthermore, a permanent part is remaining that takes more time to vanish. This viscoelastic behavior is more pronounced for shear forces, for which the capacitance signal shows a small delay to the force signal. Especially for the unloading, the capacitance follows tens of seconds after the force signal. Again, a remaining part of the capacitance signal can be observed.

The response of the capacitance to different forces is investigated. For all the following plots, the solid lines represent the loading of the sensor and the dashed lines show the unloading response. To minimize errors in measurements and reduce noise, the 16 capacitance values which were measured immediately before a change in applied force have been considered in the analysis. Figure 10 shows that the response of the sensor is linear to the normal force, and it can be seen that the hysteresis is small. The sensitivity is approximately 5.2 ± 0.3 fF/N, which is rather small. The reason lies at the large area of the sensor. The area where the

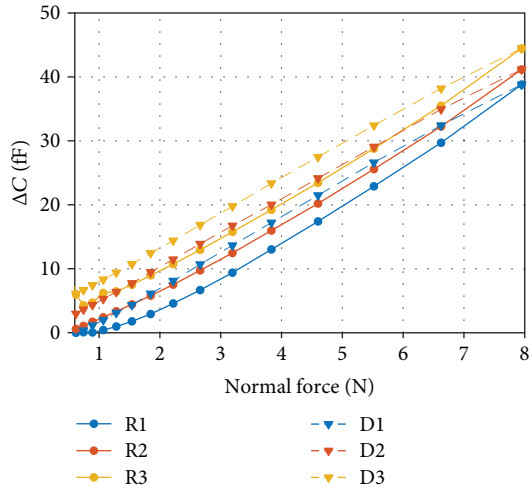

FIGURE 10: Characteristic of the sensor to three increasing (R: solid) and decreasing (D: dashed) cycles of normal force. A linear behavior was found. The drift of the signal can be explained by viscoelastic behavior of the PDMS and is reversed after a longer resting time.

PDMS was printed is approximately 2.5 × 2.5 cm^2 large, so that the maximal pressure was only about 12.8 kPa. Thus, the sensitivity to pressure is about 3.25 fF/kPa. As we only characterized one quarter of the sensor, the sensitivity for the full sensor would be four times higher, meaning 20.8 ± 0.6 fF/N or 13 fF/kPa. These values are slightly higher than in the work of Dobrzynska and Gijs [25], which achieved about 11 fF/kPa. The measured curve indicates that higher pressures would still produce higher changes in capacitance, but we were limited by our setup. Especially towards the higher force region, out sensor is linear in comparison to other sensors presented in the literature [25], and we expect that the linear region extends to a much higher force. Eventually, however, the sensor's capacitance values will saturate. The sensor's response is small and allows an accurate force

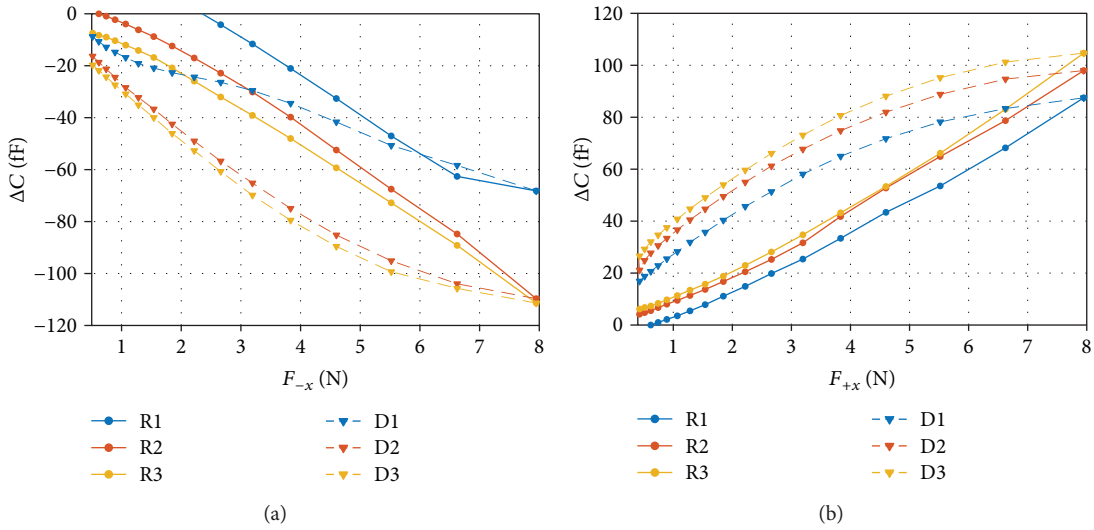

Figure 11: Characteristic of the sensor to three increasing (R) and decreasing (D) cycles of shear force in (a) $-x$-direction and (b) $+x$-direction. After the first force application, a linear behavior with a large hysteresis was found. The drift of the signal can be explained by viscoelastic behavior of the PDMS and is reversed after a longer resting time.

measurement with a temporal resolution in the order of seconds. The overall size in capacitance can be increased by increasing the area or lowering the thickness of the dielectric.

Figure 11 shows all measured values for forces in both $+x$- and $-x$-direction. The markers visualize every measured force value, which was kept for about 5 s, and the average force and capacitance values of the last four sampling points are marked. The blue markers show the first-force cycle, red the second, and yellow the third. Each rising (R) edge is shown by round markers connected by a solid line, and each decreasing (D) edge by triangular markers interconnected by a dashed line. The first measurement cycle is shown in blue in Figure 11(a) and deviates much from all other cycles. This is the reason why we decided to neglect it. Anyway, it must be shown to highlight the importance that the sensor may not work immediately as intended but may require one or more priming cycles. The following two cycles are close, with a slight drift towards lower capacitance values. This was observed for both positive and negative shear forces as well as for normal forces and is probably caused by viscoelastic deformations of the dielectric spacer PDMS. Our measurement times of only 5 s per point are rather short and does not allow the PDMS to completely adapt to the exerted force This may also be the reason for the large hysteresis with a width of up to 1.5 N. We expect that a longer measurement time would increase the absolute capacitance values of the rising edges and decrease the ones of the decreasing edges and decrease the hysteresis. Then, the capacitance values in respect to the force would follow a linear relation with a sensitivity between 12.3 ± 0.2 fF/N for the $+x$-direction and 13.8 ± 0.2 fF/N for the $-x$-direction. When the full sensor would be built, this would double to about 26 ± 0.4 fF/N because two capacitors will contribute to the measurements. Both shear-force sensitivities are similar and are about twice of the sensitivity values of the sensor in the work of Dobryzynska and Gijs [25], which was built similarly but without printing techniques.

The capacitance values of the sensors are considerably lower than the theoretical values. From the profilometer measurement, we know that the thickness of the PDMS layer is about 40 μm, and the area of the electrodes is about 44.4 mm^2. The theoretical capacitance value for 50% overlap is 12.3 pF. Our measured capacitance value was 6.82 pF and only half of the theoretical value. This capacitance would correspond to a distance of 96.8 μm. When checking the overlap of our sensor, we found that the overlap in resting state of about two-thirds (67%) was slightly higher than the desired value as can be seen in Figure 12(a) by the red-marked areas. This should lead to an even higher capacitance value of 16.5 pF. This significant deviation of the capacitance value originates most probably from some trapped air between the top electrode and the stencil-printed PDMS layer. Such trapped air bubbles are colored in red in the microscope images in Figure 12(b) and increase the average distance, but do not explain a factor of 2.5. Additionally, the lower relative permittivity of air (compared to PDMS) decreases the overall capacitance. The trapped air acts like a second capacitance connected in series. The capacitance as a function of the fraction of air $\chi = d_2/d$ and $d = d_1 + d_2$ is

$$C = \frac{\varepsilon_0 \varepsilon_r A}{d(1 - \chi + \varepsilon_r \chi)}. \quad (6)$$

Here, d is the total distance of the electrodes, d_1 denotes the thickness of the PDMS layer, and d_2 is the thickness of the air gap. For example, if the spacer contains 25% air and 75% PDMS the capacitance is reduced to 72.8% of its ideal value ($\chi = 0$, no trapped air). The combination of the higher distance due to trapped air and a lower effective permittivity leads to a reasonable relation of capacitance and distance.

The change in capacitance is originated by a displacement Δd of the top electrode with respect to the bottom

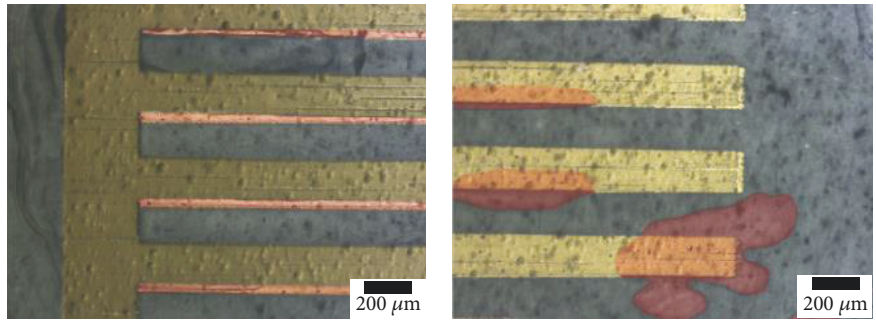

(a) (b)

Figure 12: (a) Overlapping area of the electrodes colored in red onto an optical microscope picture and (b) trapped air in the PDMS layer colored in red as well as for better visibility.

electrode. Using the distances in Table 1, we calculated the change in distance for each of the four possibilities that results in the measured change in capacitance of about 45 fF. The range of the calculated distance changes of less than a micrometer is reasonable since PDMS has a Poisson's ratio of almost 0.5 [28]. Therefore, the PDMS is only a little compressible as the lateral expansion is limited.

4. Discussion

In this work, a fully flexible, capacitive force sensor for two-axial force measurements has been developed by applying printed electronic technologies on a polymeric film. We successfully fabricated structured silver electrodes on PET foil by inkjet printing. We achieved a resolution with lines below 60 μm and an average thickness of about 500 nm. For a conducting layer, the inkjet-printed samples required an additional postproduction treatment. With photonic sintering, an ultrafast, selective, and cheap method was used to functionalize the thin films. PDMS, which was chosen for its good process ability and elastic properties, was found unsuitable for direct inkjet printing. Oxygen plasma treatment could be an effective way to overcome the hydrophobic surface properties of PDMS. Further research is required here. The most challenging task was to fabricate the stacked structure of a printed bottom electrode, a dielectric spacer, and a printed top electrode. The method of gluing the two printed sheets together to solve the problem was the best available. The main objective of this report to fabricate a printed normal and shear force sensor was achieved. By integrating this sensor into a 2-by-2 arrangement of four sensors, simultaneous normal and shear forces (three-axial) can be measured. Due to trapped air in the dielectric spacer, the experimental capacitance values were distinctly lower than the theoretical predictions.

In the force range of 0.1 to 8 N, we could find a linear relationship between the capacitance values and the exerted normal and shear forces. For normal forces, a sensitivity of 5.2 fF/N was determined and for shear forces, it was 13.1 fF/N. These values were measured only for one-quarter of the sensor of an area of about 80 mm^2. When employing four of the sensors in a different orientation, the shear force sensitivity can be doubled to 26.2 fF/N, and the normal force sensitivity quadrupled to 20.8 fF/N. These are comparable to other sensors in literature and have the main advantage that only printing techniques are employed. Only additive deposition techniques were used and the only difficult step is the alignment of both electrodes. The reduction of the finger width to the planned 60 μm or eventually 40 μm would either allow more fingers or a smaller sensor. The first would have an approximate increase of the sensitivity closer to the picofarad region. The second would decrease the area and increase the sensitivity with respect to forces as the local pressures are higher. Another improvement could be the use of structured dielectrics as in the previous section to reduce the stiffness of the dielectric. All of the materials and methods used here are low-cost and cause a very small amount of chemical waste, especially when compared to conventional semiconductor processes. This allows the production of sensors on large and flexible substrates as they are needed for artificial skins. Such skins may be employed in advanced humanoids as well as for patients without sensing capabilities on parts of their body.

Table 1: Comparison of the theoretical and measured capacitance values C_0 and their change ΔC_0, the thickness of the dielectric spacer $d_{0,}$ and the deflection Δd. Bold values are calculated from the other columns.

	C_0 (pF)	ΔC_0 (fF)	Overlap	ε_r	d_0 (μm)	Δd (nm)
Ideal 50%	**12.3**	45	50%	2.5	40.0	**146**
Ideal 67%	**16.5**	45	67%	2.5	40.0	**109**
Sensor	6.82	45	67%	2.5	**96.8**	**635**
S (25% air)	6.82	45	67%	**1.8**	**69.7**	**457**

Data Availability

The data used to support the findings of this study are available from the corresponding author upon request.

Conflicts of Interest

The authors declare no conflict of interest.

Authors' Contributions

A. Albrecht and P. Lugli contributed in the conceptualization of the study. A. Albrecht created the methodology, wrote and prepared the original draft, and did the visualization of the study. P. Lugli, M. Becherer, and M. Trautmann gathered resources. A. Rivadeneyra, P. Lugli, and M. Becherer wrote, reviewed, and edited the paper. P. Lugli and A. Rivadeneyra supervised the study. P. Lugli and M. Becherer acquired the funds for the study.

Acknowledgments

The authors want to thank Prof. Cheng of the Technical University of Munich (TUM) for the use of their lab to produce the inkjet-printed patterns used in this work and Prof. Wagner of the same university for the use of their workshop to build the two force setups. This work was partially supported by the Deutsche Forschungsgemeinschaft (DFG) within the German Excellence Initiative through the cluster of excellence "Nanosystems Initiative Munich" (NIM) and the Technical University of Munich (TUM) Graduate School.

References

[1] D. Lupo, W. Clemens, S. Breitung, and K. Hecker, "OE-A roadmap for organic and printed electronics," in *Applications of Organic and Printed Electronics*, Integrated Circuits and Systems, E. Cantatore, Ed., Springer, Boston, MA, USA, 2013.

[2] G. Nisato, D. Lupo, and S. Ganz, *Organic and Printed Electronics: Fundamentals and Applications*, CRC Press, 2016.

[3] M. Nir, D. Zamir, I. Haymov, and L. Ben-Asher, "Electrically conductive inks for inkjet printing," in *The Chemistry of Inkjet Inks*, S. Magdassi, Ed., pp. 225–254, 2010.

[4] A. Albrecht, M. Trautmann, M. Becherer, P. Lugli, and A. Rivadeneyra, "Multi-layer printed shear force sensor on flexible substrates," in *ALLSENSORS 2018, The Third International Conference on Advances in Sensors, Actuators, Metering and Sensing*, pp. 70–75, Rome, Italy, 2018.

[5] A. Albrecht, *Printed Sensors for the Internet of Things*, Technische Universität München, 2018.

[6] E. S. Hwang, J. H. Seo, and Y. J. Kim, "A polymer-based flexible tactile sensor for both normal and shear load detections and its application for robotics," *Journal of Microelectromechanical Systems*, vol. 16, no. 3, pp. 556–563, 2007.

[7] R. Pfeifer, M. Lungarella, and F. Iida, "The challenges ahead for bio-inspired 'soft' robotics," *Communications of the ACM*, vol. 55, no. 11, p. 76, 2012.

[8] N. Lu and D.-H. Kim, "Flexible and stretchable electronics paving the way for soft robotics," *Soft Robotics*, vol. 1, no. 1, pp. 53–62, 2014.

[9] R. S. Dahiya, P. Mittendorfer, M. Valle, G. Cheng, and V. J. Lumelsky, "Directions toward effective utilization of tactile skin: a review," *IEEE Sensors Journal*, vol. 13, no. 11, pp. 4121–4138, 2013.

[10] R. S. Dahiya, G. Metta, M. Valle, and G. Sandini, "Tactile sensing-from humans to humanoids," *IEEE Transactions on Robotics*, vol. 26, no. 1, pp. 1–20, 2010.

[11] J. A. Rogers, T. Someya, and Y. Huang, "Materials and mechanics for stretchable electronics," *Science*, vol. 327, no. 5973, pp. 1603–1607, 2010.

[12] T. Sekitani and T. Someya, "Stretchable organic integrated circuits for large-area electronic skin surfaces," *MRS Bulletin*, vol. 37, no. 3, pp. 236–245, 2012.

[13] G. Schwartz, B. C. K. Tee, J. Mei et al., "Flexible polymer transistors with high pressure sensitivity for application in electronic skin and health monitoring," *Nature Communications*, vol. 4, no. 1, p. 1859, 2013.

[14] M. Kaltenbrunner, T. Sekitani, J. Reeder et al., "An ultra-lightweight design for imperceptible plastic electronics," *Nature*, vol. 499, no. 7459, pp. 458–463, 2013.

[15] A. Albrecht, A. Rivadeneyra Torres, J. F. Salmerón, A. Abdellah, and P. Lugli, "Inkjet printing and photonic sintering of silver and copper oxide nanoparticles for ultra-low-cost conductive patterns," *Journal of Materials Chemistry C*, vol. 4, no. 16, pp. 3546–3554, 2016.

[16] W. Y. Chang, T. H. Fang, H. J. Lin, Y. T. Shen, and Y. C. Lin, "A large area flexible array sensors using screen printing technology," *IEEE/OSA Journal of Display Technology*, vol. 5, no. 6, pp. 178–183, 2009.

[17] C. L. Choong, M. B. Shim, B. S. Lee et al., "Highly stretchable resistive pressure sensors using a conductive elastomeric composite on a micropyramid array," *Advanced Materials*, vol. 26, no. 21, pp. 3451–3458, 2014.

[18] R. S. Dahiya and M. Valle, *Robotic Tactile Sensing : Technologies and System*, Springer, 2013.

[19] M. R. Cutkosky, R. D. Howe, and W. R. Provancher, "Force and tactile sensors," in *Springer Handbook of Robotics*, B. Siciliano and O. Khatib, Eds., pp. 455–476, Springer, Berlin, Heidelberg, 2008.

[20] H.-K. Lee, J. Chung, S.-I. Chang, and E. Yoon, "Normal and shear force measurement using a flexible polymer tactile sensor with embedded multiple capacitors," *Journal of Microelectromechanical Systems*, vol. 17, no. 4, pp. 934–942, 2008.

[21] S. C. B. Mannsfeld, B. C. K. Tee, R. M. Stoltenberg et al., "Highly sensitive flexible pressure sensors with microstructured rubber dielectric layers," *Nature Materials*, vol. 9, no. 10, pp. 859–864, 2010.

[22] T. A. T. A. Chase and R. C. R. C. Luo, "A thin-film flexible capacitive tactile normal/shear force array sensor," in *Proceedings of IECON '95-21st Annual Conference on IEEE Industrial Electronics*, pp. 1196–1201, Orlando, FL, USA, 1995.

[23] S. Khan, L. Lorenzelli, and R. S. Dahiya, "Screen printed flexible pressure sensors skin," in *25th Annual SEMI Advanced Semiconductor Manufacturing Conference (ASMC 2014)*, pp. 219–224, Saratoga Springs, NY, USA, 2014.

[24] L. Viry, A. Levi, M. Totaro et al., "Flexible three-axial force sensor for soft and highly sensitive artificial touch," *Advanced Materials*, vol. 26, no. 17, pp. 2659–2664, 2014.

[25] J. A. Dobrzynska and M. A. M. Gijs, "Polymer-based flexible capacitive sensor for three-axial force measurements," *Journal of Micromechanics and Microengineering*, vol. 23, no. 1, article 015009, 2013.

[26] R. Surapaneni, Q. Guo, Y. Xie, D. J. Young, and C. H. Mastrangelo, "A three-axis high-resolution capacitive tactile imager system based on floating comb electrodes," *Journal*

of Micromechanics and Microengineering, vol. 23, no. 7, article 075004, 2013.

[27] J. E. Mark, *Polymer Data Handbook*, Oxford University Press, 2009.

[28] S. Yao and Y. Zhu, "Nanomaterial-enabled stretchable conductors: strategies, materials and devices," *Advanced Materials*, vol. 27, no. 9, pp. 1480–1511, 2015.